Journal of Hazardous Materials 420 (2021) 126528

Contents lists available at ScienceDirect

Journal of Hazardous Materials

journal homepage: www.elsevier.com/locate/jhazmat

Research Paper

Lead (Pb) sorption to hydrophobic and hydrophilic zeolites in the presence and absence of MTBE

Yunhui Zhang [a,b,c,d], Daniel S. Alessi [d,*], Ning Chen [e], Mina Luo [f], Weiduo Hao [d], Md. Samrat Alam [d,g], Shannon L. Flynn [h], Janice P.L. Kenney [i], Kurt O. Konhauser [d], Yong Sik Ok [j], Abir Al-Tabbaa [c]

[a] College of Environmental Science and Engineering, Tongji University, Shanghai 200092, China
[b] State Key Laboratory of Pollution Control and Resource Reuse, Tongji University, Shanghai 200092, China
[c] Department of Engineering, University of Cambridge, Cambridge CB2 1PZ, United Kingdom
[d] Department of Earth and Atmospheric Sciences, University of Alberta, Edmonton T6G 2E3, Canada
[e] Canadian Light Source Inc., University of Saskatchewan, 114 Science Plane, Saskatoon, Saskatchewan S7N 0X4, Canada
[f] College of Chemistry and Chemical Engineering, Southwest Petroleum University, Chengdu 610500, China
[g] Department of Earth Sciences, University of Toronto, 22 Russell Street, Toronto, ON M5S 3B1, Canada
[h] School of Natural and Environmental Science, Newcastle University, Newcastle upon Tyne NE1 7RE, United Kingdom
[i] Department of Physical Sciences, MacEwan University, Edmonton, Alberta T5J 2P2, Canada
[j] Korea Biochar Research Center, APRU Sustainable Waste Management Program & Division of Environmental Science and Ecological Engineering, Korea University, Seoul, Republic of Korea

ARTICLE INFO

Editor: Dr. H. Artuto

Keywords:
Clean water and sanitation
Sorbent
Surface coating
Zeolite
Advanced spectroscopic analysis

ABSTRACT

The co-contamination of the environment by metals and organic pollutants is a significant concern, and one such example is lead (Pb) and methyl tert-butyl ether (MTBE) due to their historic use as fuel additives. Clinoptilolite is an abundant and efficient zeolite for metal removal, but the potential interference of co-existing organic pollutants on metal removal, such as MTBE, have rarely been discussed. In this study, a combination of batch sorption tests and synchrotron-based X-ray absorption spectroscopic analyses were employed to investigate Pb sorption mechanism(s) onto clinoptilolite in the presence and absence of MTBE. A comparison was made to synthetic ZSM-5 zeolite to gain insights into differences in Pb binding mechanisms between hydrophilic (clinoptilolite) and hydrophobic (ZSM-5) zeolites. Site occupancy and surface precipitation contributed equally to Pb removal by clinoptilolite, while surface precipitation was the main Pb removal mechanism for ZSM-5 followed by site occupancy. Despite the negligible effect of 100 mg/L MTBE on observed Pb removal from solution by both zeolites, a surface-embedded Pb removal mechanism, through the Mg site on clinoptilolite surface, arises when MTBE is present. This study provides an understanding of atomic-level Pb uptake mechanisms on zeolites, with and without co-contaminating MTBE, which aids in their application in water treatment at co-contaminated sites.

1. Introduction

The co-contamination of sites by both organic and inorganic contaminants is a common and complex environmental issue (Zhang et al., 2021a). The remediation of co-contaminated sites is difficult due to the differing behavior of each contaminant and often requires more than one remediation approach (Arjoon et al., 2013; Liu et al., 2018a, 2018b). One example of common inorganic and organic co-contaminant pairing is methyl-tert-butyl ether (MTBE) and Pb, both of which were used fuel additives (Zhang et al., 2019a). While the use of Pb has been phased out, MTBE remains a widespread organic contaminant due to its continued use as a petrol additive, accounting for 91.8% of its global use in 2018 (Global Industry Analysts, 2019). Due to its genotoxicity, and being an irritation to skin, eyes and respiratory systems, MTBE is considered a significant groundwater contaminant (Zhang et al., 2019b) and has been banned in a number of countries. In spite of the reduction of MTBE use as a petrol oxygenate to 18.2% in 2018, the global MTBE market remains large and is projected to reach 24.5 million tonnes by 2024 (Global Industry Analysts, 2019). Surprisingly, few studies have investigated the effects of organic contaminants, such as MTBE, on the removal of toxic

* Corresponding author.
E-mail address: alessi@ualberta.ca (D.S. Alessi).

https://doi.org/10.1016/j.jhazmat.2021.126528
Received 5 May 2021; Received in revised form 14 June 2021; Accepted 25 June 2021
Available online 29 June 2021

metals from solution by natural or synthetic sorbents.

Adsorption is a process demonstrated to be efficient in removing organic and inorganic contaminants from aqueous environments (Krauklis et al., 2017; Ozola et al., 2019). Naturally occurring zeolites are a class of common mineral adsorbents used for the removal of metals from contaminated water due to their high efficiency and low cost (Wang and Peng, 2010; Yuna, 2016). As the most abundant zeolite, clinoptilolite [$(Na,K,Ca)_{2-3}Al_3(Al,Si)_2Si_{13}O_{36}\bullet 12H_2O$] has a high adsorption capacity for heavy metals due to its hydrophilicity, large specific surface area and high cation exchange capacity (CEC) (Li et al., 2002; Mihaly-Cozmuta et al., 2014). Although many studies have examined the adsorption of heavy metals onto a wide range of zeolites, most of these studies focus on basic observations, such as adsorption kinetics and degree of metal uptake as a function of pH, ionic strength, or other environmental factors (Aghazadeh et al., 2016; Mihaly-Cozmuta et al., 2014; Sprynskyy et al., 2006). Few studies have explored the atomic-scale metal binding mechanisms at the zeolite surface (Izumi et al., 2002; Logar et al., 2006), or the impacts of co-contaminating organic pollutants on the adsorption mechanisms. In this regard, synchrotron-based extended X-ray absorption fine structure (EXAFS) spectroscopy can be used to determine the coordination environment of metals in the framework of ion-exchanged materials, including zeolites, and thereby elucidate metal adsorption mechanisms. For example, Filippousi et al. (2015) used EXAFS in Zn-exchange experiments to show that the majority of Zn^{2+} exists as single ions octahedrally coordinated with oxygen within the HEU-type zeolite. Um and Papelis (2003) studied the pH and ionic strength dependence of Pb adsorption to clinoptilolite, and using EXAFS found that Pb was adsorbed at Na1 and Ca2 cation exchange sites in a large channel with ten tetrahedral rings and a small channel with eight tetrahedral rings of clinoptilolite at low pH and low ionic strength, respectively. At the highest ionic strength (1.0 M) and low pH, Pb^{2+} formed monodentate and corner-sharing inner-sphere complexes at aluminol (Al-OH) or silanol (Si-OH) sites, while edge-sharing bidentate inner-sphere complexes form on external hydroxyl (-OH) sites at higher pH values. Moreover, mononuclear complexes are known to be systematically replaced by binuclear complexes as Pb^{2+} concentration increases. However, these studies were conducted in a single sorbent – single sorbate system without considering potential effects of co-contaminants that commonly exist at contaminated sites. Therefore, research is needed to determine the distribution of metals, such as Pb, and their local coordination geometry in the framework of zeolites with co-contaminants to better predict how organic pollutants may influence the stability of metals bound to zeolite particles.

This study aims to explore the mechanisms of Pb sorption to clinoptilolite in comparison to ZSM-5, in the presence and absence of MTBE. The study includes the following objectives: to determine (1) the protonation and deprotonation constants of surface adsorption sites, the densities of adsorption sites, and the identification of adsorption sites on clinoptilolite surfaces; (2) the aqueous adsorption behavior of Pb as a function of pH; (3) the effects of co-contaminating MTBE on Pb removal from solution; (4) the atomic coordination environments of sorbed Pb with and without the presence of MTBE; and (5) differences in Pb sorption behavior onto clinoptilolite and ZSM-5 (a common hydrophobic zeolite). Addressing these objectives will provide valuable information about the use of zeolites to treat Pb in co-contaminated environments and enhance our understanding of the mechanisms of Pb binding and stability on zeolites following their use for water treatment.

2. Materials and methods

2.1. Materials

Clinoptilolite was provided by Kentish Minerals, Westerham, Kent, UK. It is a natural HEU-type zeolite composed of hydrated calcium aluminosilicate of volcanic origin, containing a minimum 85% clinoptilolite and a maximum 15% of feldspar, micas and clays, free of fiber and quartz, as provided by the supplier. The chemical composition was 71.1% SiO_2, 11.7% Al_2O_3, 3.9% K_2O, 3.0% CaO, 0.8% Fe_2O_3, 0.7% MgO and 0.6% Na_2O with a SiO_2/Al_2O_3 molar ratio of 6.1. The pore volume was 0.34 cm^3/g and the cation exchange capacity (CEC) was 180 meq/100 g, as provided by the supplier. Upon receipt, the clinoptilolite was ground and sieved through 75 μm (200 mesh) for use. The physicochemical properties of ZSM-5 zeolite can be found in our previous study (Zhang et al., 2021b).

2.2. Characterization

The pH of clinoptilolite was measured by adding 0.1 g of clinoptilolite to 20 mL of deionised water then shaken at 200 rpm for 2 h (Shen et al., 2015). The final mixture was filtered using a 0.45 μm nylon membrane and the pH of the filtrate was measured using an Accumet AP85 pH meter. The water contact angle was measured according to the sessile drop method (Alghunaim et al., 2016) using a contact angle measuring device (KRÜSS, Germany, Germany) at the University of Alberta, Canada. Microstructural analyses, i.e., Scanning Electron Microscope with Energy Dispersive X-ray spectroscopy (SEM/EDX) and Thermogravimetry (TGA), were also conducted to examine the surface morphology and thermal decomposition of clinoptilolite, respectively.

2.3. Potentiometric titrations

Potentiometric acid-base titrations were conducted to determine the proton buffering capacity of clinoptilolite. Prior to a titration, the pH electrode (Metrohm 905 Titrando) was calibrated using a set of three pH buffers (pH 4.0, 7.0, 10.0). Approximately 0.05 g of dry clinoptilolite powder was suspended in 50 mL of 0.01 M $NaNO_3$ electrolyte solution to make a 1 g/L ZSM-5 suspension. The sample containers were then sealed with Parafilm and purged with N_2 gas for 30 min prior to titration. During titrations, the experimental apparatus remained sealed and was continually bubbled with N_2 to prevent CO_2 from entering the system. A forward titration (pH 3–11) and a reverse titration (pH 11–3) were performed for each samples to check for hysteresis in titration curves, which can be indicative of sample damage or irreversibility of proton sorption (Alessi et al., 2019a, 2019b; Duc et al., 2005). Additional information on the titration protocols can be found in our previous papers (Hao et al., 2018; 2019).

2.4. Pb sorption tests

Batch sorption equilibrium experiments were carried out with the initial lead nitrate concentrations varying from 5 to 500 mgPb/L at a zeolite to liquid ratio of 1 g/L to obtain sorption isotherms at pH 4 and 6. The ionic strength was buffered using a solution of 1 M $NaNO_3$. The effect of pH was evaluated at a total lead concentration of 40 mg/L and in increments of one pH unit between pH 3–10. The effect of co-contaminating MTBE was evaluated by the addition of 100 mg/L of MTBE in both isotherm and pH edge experiments. 100 mg/L was chosen as MTBE is reported to show acute toxicity at concentrations greater than 151 mg/L and chronic toxicity when greater than 51 mg/L in freshwater (EPA, 2006). Pb sorption on zeolites is reported to reach equilibrium within 12 h (Karatas, 2012); therefore, the supernatant was filtered through 0.20 μm nylon membranes (Millex HP) after shaking for 24 h to ensure equilibrium had been achieved. The Pb concentrations in the filtered supernatants were measured by ICP-MS/MS (Agilent 8800). All experiments were conducted in duplicate.

2.5. Extended X-ray adsorption fine spectroscopy (EXAFS) analysis

Lead *L3-edge* XAFS measurements were conducted at the Hard X-ray Micro-Analysis (HXMA) beamline of the Canadian Light Source (CLS) in Saskatoon, Canada (Jiang et al., 2007). Samples of clinoptilolite, to

which Pb was sorbed at pH 4 and at pH 6 were used for XAFS analyses. A detailed description of XAFS data collection methods can be found in the Supporting Information and our previous study (Zhang et al., 2021b). Briefly, transmission mode was used to collect spectra for the model compound, lead oxide hydrate (PbO•(H_2O)) (Tolkachev et al., 1958), and fluorescence mode was applied for the Pb sorbed clinoptilolite samples using a 32 element Ge array detector. The Pb *L3-edge* data collection configuration was set as (−200 to −30 eV; 10 eV/step, 2 s/point) for the pre-edge region; (−30 to 70 eV; 0.5 eV/step, 2 s/point) for X-ray absorption near edge structure (XANES); and (70 eV to 14 $Å^{-1}$, 0.05 $Å^{-1}$/step, 2–10 s/point) for EXAFS, respectively. Data reduction, the Feff 7 based R space curve fitting (Rehr and Albers, 2000) and XANES theoretical modeling were performed using ATHENA software (Ravel and Newville, 2005), WINXAS version 2.3 (Ressler, 1997) and the FDMNES code (Joly, 2001), respectively.

3. Results and discussion

3.1. Protonation model of the clinoptilolite

The pH of clinoptilolite in deionized water was measured to be 6.7, and the contact angle was 24.97 ± 0.65°. It is generally accepted that a surface is hydrophilic when its static water contact angle < 90° and is hydrophobic when the contact angle is > 90° (Förch et al., 2009). The hydrophilicity of clinoptilolite was further calculated (Anderson and Klinowski, 1986; Erdem-Şenatalar et al., 2004) based on the TGA pattern (Fig. S1). This calculation indicated a low hydrophobicity for clinoptilolite of 0.44 compared with 0.57 for ZSM-5 (Zhang, 2019). The morphology and elemental compositions of clinoptilolite are shown in Fig. S2 and Table S1. Surface complexation modeling (SCM) was used to model the acid-base titration data, quantify the surface adsorption site densities and determine proton interaction constants (pKa values). Both a non-electrostatic model (NEM) and constant capacitance model (CCM) were applied using the software package FITEQL 3.2 (Herbelin and Westall, 1996). When compared to a blank titration of 0.01 M $NaNO_3$ (Hao et al., 2018), clinoptilolite had a strong proton buffering capacity across the tested pH range. The experimental titration curve was fitted by both the NEM and CCM approaches (Fig. S3). The NEM has a relatively better fit compared to CCM based on V_Y values. The calculated parameters resulting from titration curve fitting are given in Table 1, where ≡XH represents ion exchange sites generated by isomorphic substitution in the zeolite structure, and ≡SOH represents amphoteric basal sites, either ≡AlOH or ≡SiOH, at the zeolite surface.

3.2. Sorption of Pb on clinoptilolite

3.2.1. Sorption isotherms

The experimental sorption isotherm data were fit using both the Langmuir and Freundlich models (Fig. S4 and Table 2). Although both models adequately described the Pb sorption on clinoptilolite with high correlation coefficients ($R^2 > 0.84$ and $p < 0.01$), the sorption of Pb onto clinoptilolite was better fit by the Freundlich model at both pH 4 and 6, as assessed by higher R^2 values and lower Akaike information criterion (AIC) values (Zhang et al., 2018a). The sorption capacity of clinoptilolite at pH 6 was higher than at pH 4. It should be noted that the precipitation of lead carbonate was not predicted to occur under experimental conditions, even when considering the solutions in equilibrium with atmospheric CO_2 (Zhang et al., 2021b). Speciation modeling (Fig. S5) shows that lead hydroxide was the favored precipitate at higher pH, leading to higher Pb removal from solution at alkaline pH (Zhang et al., 2018b). As compared in Table 2, the Pb sorption capacity of the hydrophilic clinoptilolite was found to be considerably higher the tested hydrophobic zeolite, ZSM-5, under the same experimental conditions reported in our previous study (Zhang et al., 2021b). This is reasonable because clinoptilolite has a much lower Si/Al ratio and, therefore, more free cations to exchange with lead ions, resulting in a higher sorption capacity.

Table 1
Calculated parameters from the protonation model of titration data of clinoptilolite.

Models	Parameters	≡XH ↔ ≡X^- + H^+	≡SOH ↔≡SO^- + H^+	≡SOH + H^+ ↔≡SOH_2^+
NEM	pK_a	6.92	10.13	–9.74
	Site density (mol/g)	1.51×10^{-5}	6.53×10^{-5}	
	V_Y (variance)	1.14194		
CCM	pK_a	7.31	11.64	–9.88
	Site density (mol/g)	1.07×10^{-5}	6.40×10^{-5}	
	Surface area (m^2/g)	29.3		
	Inter-layer capacitance (F/m^2)	7[a]		
	V_Y (variance)	12.92771		

[a] Inter-layer capacitance was assumed to be the same as clay minerals that have been previously published (Hao et al., 2020; Liu et al., 2018a, 2018b).

Table 2
Isotherm model parameters for Pb sorption on clinoptilolite in comparison with ZSM-5.

Models	Parameters	pH 4		pH 6	
		Clinoptilolite	ZSM-5	Clinoptilolite	ZSM-5
Langmuir	Q_0 (mg/g)	95.48 ± 15.93	14.39 ± 5.83	108.31 ± 12.85	46.34 ± 6.25
	b (L/mg)	0.01 ± 0.01	0.009 ± 0.006	0.04 ± 0.02	0.016 ± 0.004
	R_L	0.14	0.991	0.05	0.984
	AIC	49.44	20.04	61.58	25.74
	p	0.002	0.002	1.57×10^{-5}	2.05×10^{-4}
	R^2	0.89	0.97	0.84	0.99
Freundlich	K_F (mg/g)	8.64 ± 1.65	0.16 ± 0.10	20.88 ± 2.99	1.12 ± 0.25
	1/n	0.38	0.81	0.28	0.72
	AIC	39.86	21.64	47.61	27.10
	p	1.18×10^{-4}	0.003	6.53×10^{-8}	3.07×10^{-4}
	R^2	0.98	0.96	0.96	0.99

3.2.2. Effect of pH and presence of MTBE

The sorption of Pb to clinoptilolite increased from approximately 65–70% over the pH range of 3–5 and to 100% by pH 7 and higher (Fig. 1). The trend of increasing Pb sorption with the increase solution pH is more enhanced for ZSM-5, with the sorption increasing from < 10% at pH 5.5–100% at and above pH 7 (Zhang et al., 2021b). MTBE was found to have a negligible effect on Pb sorption on both zeolites because MTBE primarily enters the pores of zeolites (Zhang et al., 2018a).

3.3. EXAFS investigation

To gain a better understanding of sorption mechanisms, synchrotron-based Pb *L3-edge* EXAFS analyses were performed to investigate the local atomic environment of sorbed Pb onto clinoptilolite in the absence and presence of MTBE.

3.3.1. Structural models developed for EXAFS analysis

As introduced in our previous study on Pb sorption to ZSM-5 zeolite (Zhang et al., 2021b), the M-1 model was developed to represent the PbO•(H_2O) type of Pb surface coating on zeolite, and the M-2 model was developed to describe a second possible Pb bearing mechanism, i.e., surface Pb to Si site occupancy. The M-3 model was developed by combining features of the M-1 with M-2 models. These three models were used in the R space fitting of spectra collected from samples of

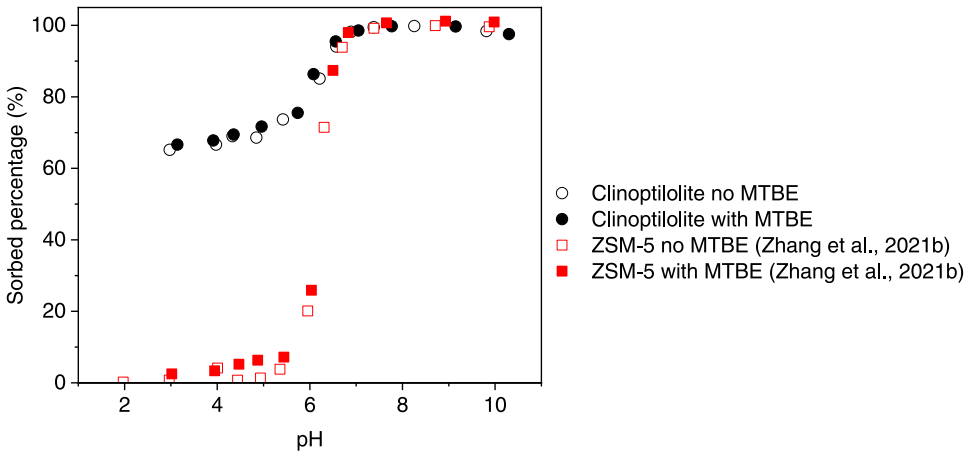

Fig. 1. Sorption edge plots of Pb sorption on clinoptilolite in the presence and absence of MTBE and its comparison with ZSM-5 (Zhang et al., 2021b).

Pb-sorbed clinoptilolite at pH 6 in the absence (Fig. 2) and presence of MTBE (Fig. 3). The experimental data and fitting results are shown in Table 3. Fig. 2a shows the comparison between experimental data and Feff modeling based fit in terms of magnitude of Fourier transform (FT) and the imaginary part of the FT, while Fig. 2b shows the comparison among the magnitude of FT of experimental data and total Feff for all fitted scattering paths and Feff for each individual scattering paths. The comparison for $k^3\chi(k)$ was further made between the experimental data and the R space curve fitting based on Feff modeling in Fig. 2c, and between experimental data and R space fitting based total Feff modeling and each fitted individual scattering path in Fig. 2d. The M-3 model guided EXAFS R space curve fitting (black dashed line, Fig. 2a) accurately describes the experimental data (black solid line, Fig. 2a) for sorption of Pb in the absence of MTBE. However, the M-3 model cannot fully address the dual peak structure of the first FT peak (red dashed box in Fig. 3a) for this system. Additionally, Feff modeling based on the M-3 model-constrained R space curve has an inverse in oscillation phase for the EXAFS in the latched experimental data at around 9 $Å^{-1}$ (Fig. 3c). Therefore, the M-4 model was developed based on the structure of clinoptilolite to guide further R space fitting of Pb sorption in the presence of MTBE. The M-4 model invokes a surface-embedded type of Pb uptake mechanism through the Mg site on the clinoptilolite surface.

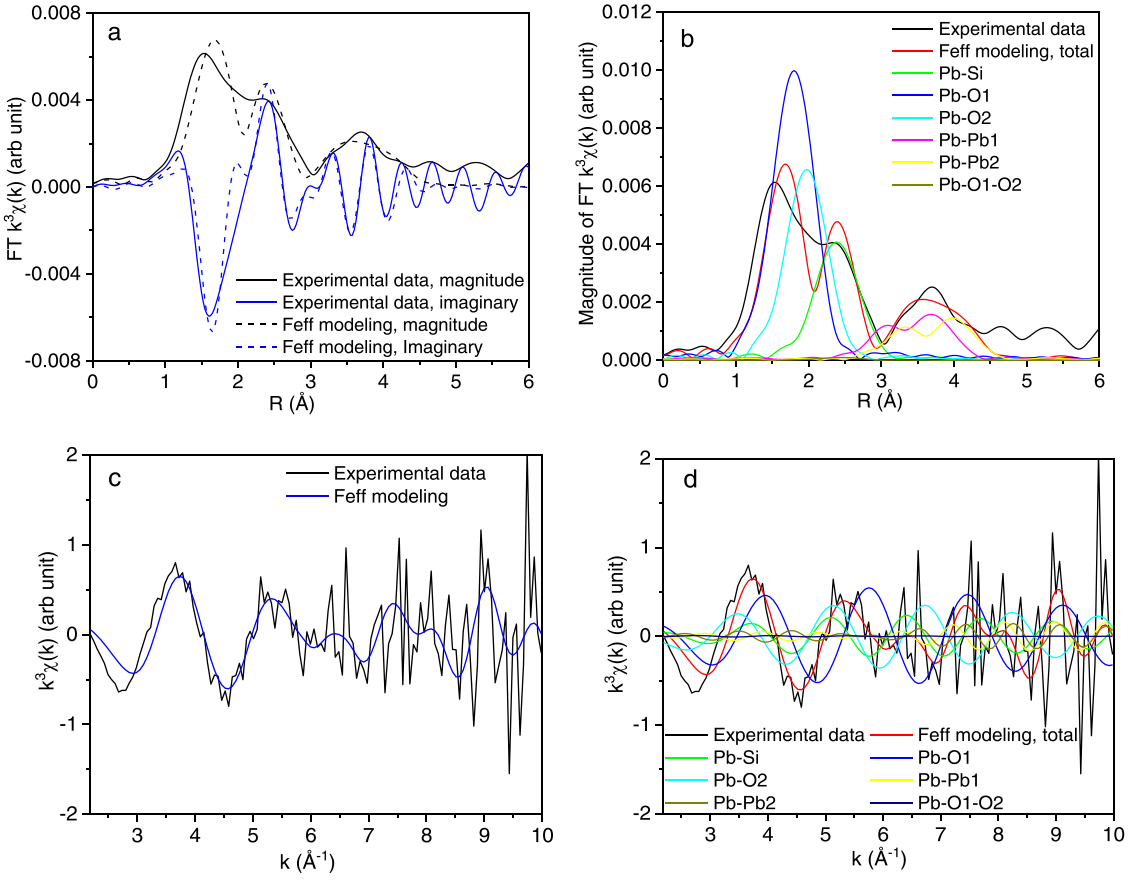

Fig. 2. Comparison of experimental data for Pb sorption onto clinoptilolite at pH 6 in the absence of MTBE and Feff modeling based fit by the M-3 model in terms of magnitude of FT and the imaginary part of the FT (a); comparison among the magnitude of FT of experimental data, total Feff for all fitted scattering paths and Feff for each individual scattering paths (b); $k^3\chi(k)$ (c) and experimental data, R space fitting based total Feff modeling and each fitted individual scattering path (d).

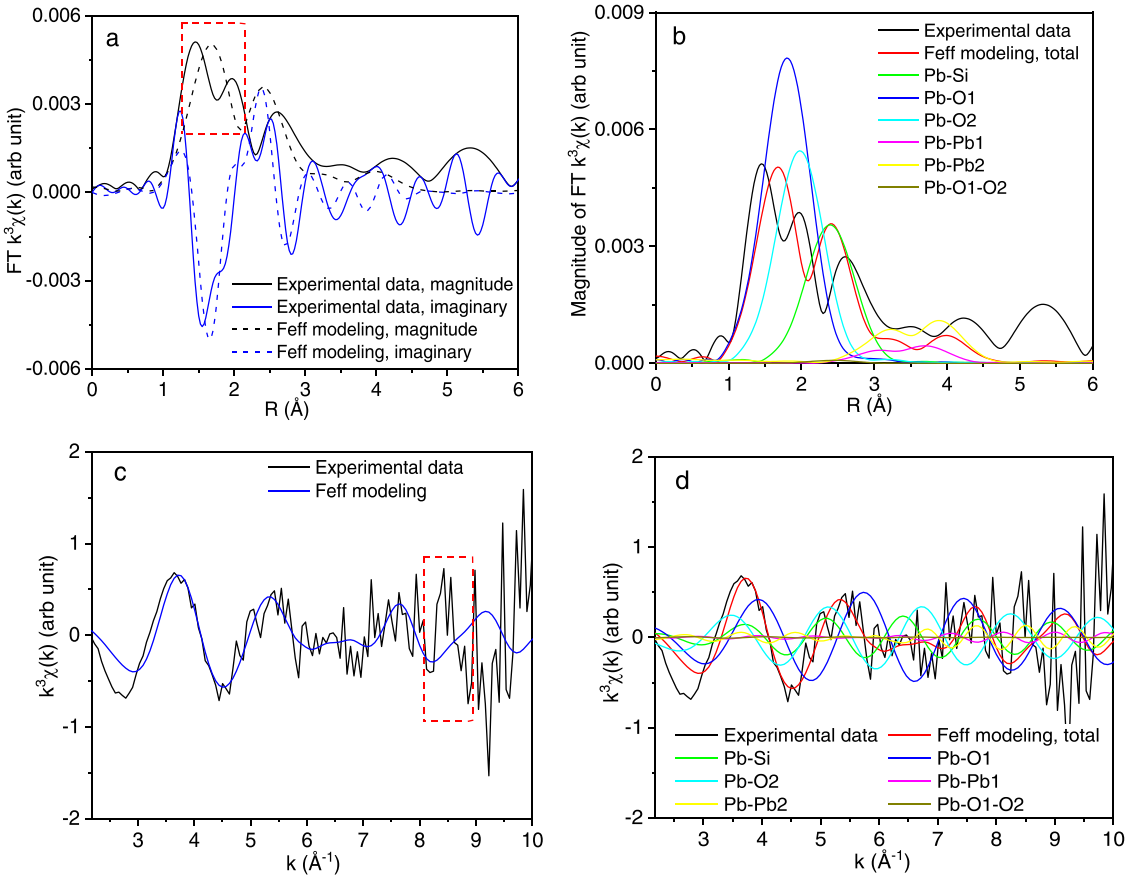

Fig. 3. Comparison of experimental data for Pb sorption onto clinoptilolite at pH 6 in the presence of MTBE and Feff modeling based fit by the M-3 model in terms of magnitude of FT and the imaginary part of the FT (a); Comparison among the magnitude of FT of experimental data, total Feff for all fitted scattering paths and Feff for each individual scattering paths (b); $k^3\chi(k)$ (c) and experimental data, R space fitting based total Feff modeling and each fitted individual scattering path (d).

Table 3
Pb L3 edge R space curve fitting results for Pb sorption onto clinoptilolite at pH 6 with or without MTBE.

Path/sub-model	M-3 model			Without MTBE				With MTBE			
	Paths	CN	R (Å)	CN	R (Å)	σ^2 (Å^2)	E_0 (eV)	CN	R (Å)	σ^2 (Å^2)	E_0 (eV)
1 (M-1)	Pb-Si	2	3.07	0.6	2.93	0.0068	–6.0	0.6	2.93	0.0068	–6.0
2 (M-2)	Pb-O1	3	2.32	1.3	2.32	0.0050		1.2	2.33	0.0050	
3 (M-2)	Pb-O2	1	2.57	1.1	2.52	0.0050		1.0	2.52	0.0050	
4 (M-2)	Pb-Pb1	2	3.98	0.8	3.78	0.0068		0.3	3.78	0.0068	
5 (M-2)	Pb-Pb2	4	4.14	1.4	4.09	0.0104		1.1	3.98	0.0100	
6 (M-2)	Pb-O-O	4	4.34	0.4	3.26	0.0070		0.4	3.26	0.0070	

3.3.2. *EXAFS characterization*

The crystallographic information file (CIF) of clinoptilolite is ICSD-66458, and its framework is presented in Fig. 4. The hatched region in Fig. 4a is the Mg site with a site occupancy of 0.08. As shown in the hatched region in Fig. 4b, when the Mg site is unoccupied, the coordination of the Mg site is determined by the occupancy of neighboring Na1 sites (occupancy 0.32), Na2 sites (occupancy 0.74) and K sites (occupancy 0.07), as shown in Fig. 4c. If the Na1, Na2 and K sites are fully occupied, the Mg site is 12-fold coordinated by oxygen as shown in Fig. S6. The 1st, 2nd and 3rd sub shells of the Mg site correspond to oxygen bonding defined by the Na1, Na2 and K sites, respectively. It would be unphysical if the Na1, Na2 and K sites are simultaneously occupied. The Mg-O distance of the 1st subshell coordination in Figs. S6 and S7a indicates that only the Na1 site is fully occupied on both sides of the Mg site (one of two sides shown in Fig. 4c). The Mg-O distance of the 2nd sub shell coordination (Figs. S6 and S7b) means that the Na1 and Na2 sites are fully occupied on both sides of the Mg sites (Fig. 4c). All three sub shells are developed when the K sites are also fully occupied on both sides of the Mg sites (Fig. 4, S6 and S7c).

Fig. 5 shows the Feff R space curve fitting for the experimental data in relation to Pb sorption onto clinoptilolite in the presence of MTBE, guided by the Feff k space modeling in the M-4 model. The R space curve fitting results based on the M-4 model are presented in Table 4. Fig. 5a compares the experimental data and Feff modeling in terms of magnitude of FT (black lines) and the imaginary part of FT (blue lines), where the solid lines and dashed lines represent the experimental data and the Feff modeling, respectively. The inverse trend at approximately 9 Å in Fig. 3c, which cannot be addressed by the M-3 model, is best described by the M-4 model as shown in Fig. 5c. The outer shell FT peaks in the range of 4–6 Å in Fig. 5a were not fit due to the low data quality. Pb-O1, Pb-O2 and Pb-O3 correspond to coordination to oxygen at the Na1 site (1st sub shell), Na2 site (2nd sub shell), and K3 site (3rd sub shell), respectively (Table 4). It is shown that the Pb-O1 coordination in the M-4 model does not describe the experimental data, suggesting that the neighboring Na1 site is not occupied if the Mg site is occupied by Pb. Fitting does resolve a Pb-O2 coordination using the M-4 model at 1.82 Å,

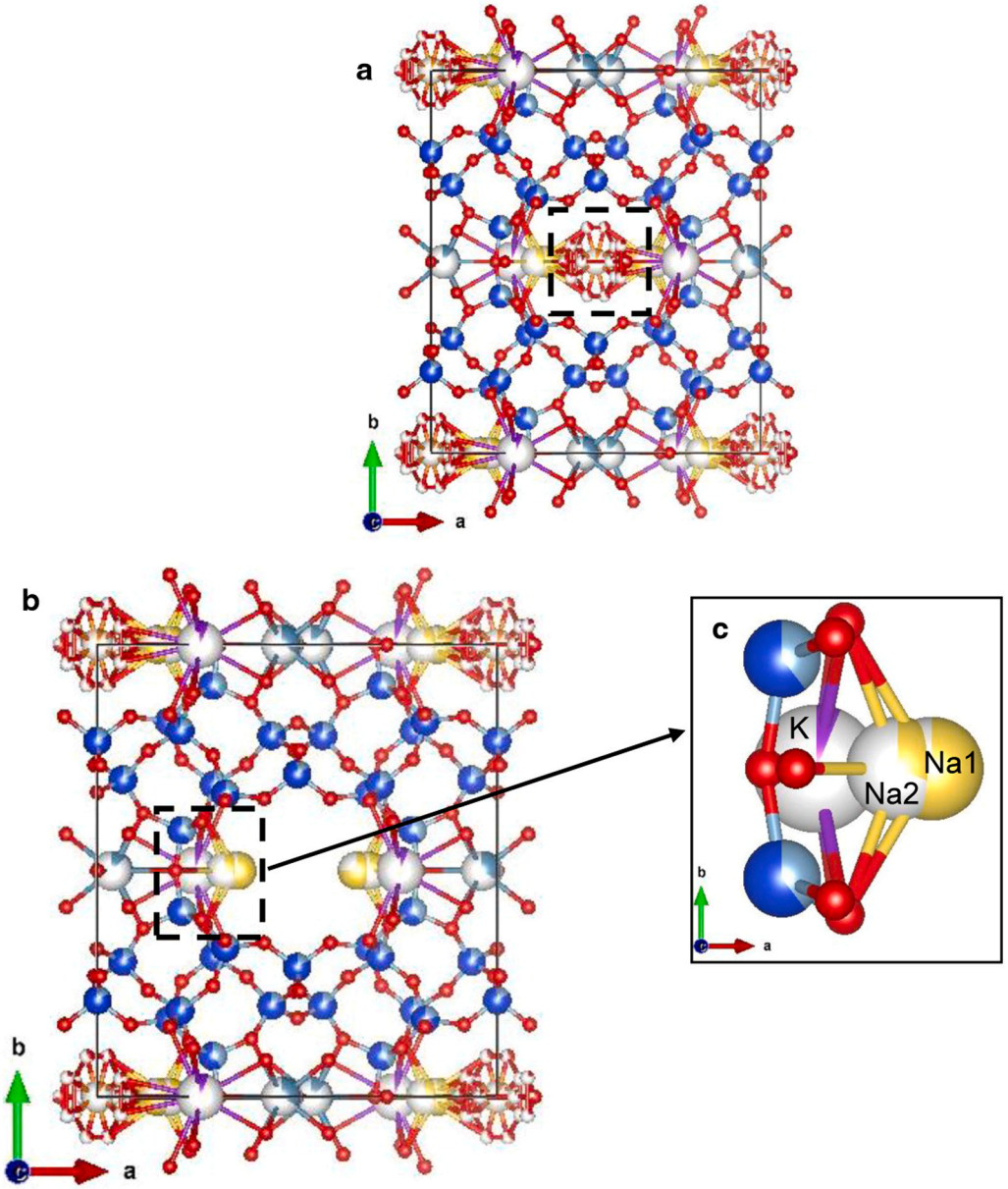

Fig. 4. Framework of clinoptilolite with the Mg site occupied (a) or unoccupied (b), and a detailed view of Na1, Na2 and K sites (c).

which is different from the Pb-O paths specified by the M-2 model (Zhang et al., 2021b). This result reveals that an additional Pb species is needed to explain the coordination of Pb sorbed in the presence of MTBE. This Pb-O2 scattering path corresponds to the 2nd subshell Mg site Pb-O coordination (Fig. 5b), thus suggesting a Pb-Na2 paired occupancy. This result is reasonable due to the fact that the Na2 site has the highest occupancy rate of the sites (0.74 for Na2 site, 0.32 for Na1 site and 0.07 for K site). However, the fitted CN for this path was relatively low (0.3), suggesting that M-4 type Pb species are secondary in this sorption system. That is, surface-embedded Pb uptake at Mg sites of the clinoptilolite surface was a secondary mechanism when MTBE was present.

The Mg site is a candidate surface site for Pb occupancy through an "embedded" uptake mechanism, but only: (a) when the Mg site is vacant; (b) when the site is exposed on the clinoptilolite surface; (c) before the formation of lead hydroxide (M-1 type); and (d) when the Na2 site is occupied. It should be noted that the Pb-Na2 site occupancy is likely to be a point of nucleation of $PbO•(H_2O)$ particles, which has a role similar to that of the Pb-Si site occupancy for Pb sorption onto ZSM-5 (Zhang et al., 2021b). Therefore, the M-3 model best describes the main Pb uptake mechanism on clinoptilolite in the presence of MTBE. The fitted Pb-O3 coordination of the M-4 model (R = 2.42 Å; Table 4) may be related to the M-2 model, i.e., an averaging effect from Pb-O1 and Pb-O2 of the M-2 model, rather than the specific M-4 model. Therefore, site occupancy and surface precipitation described by the M-3 model constitute the main Pb uptake mechanism, and the surface "embedded" Pb uptake through the Mg site on the surface comprises the secondary mechanism that is active in the presence of MTBE.

Overall, the EXAFS features of the Pb-clinoptilolite system are explained by the M-3 model, while the M-4 model is required to address the EXAFS features of the Pb-clinoptilolite-MTBE system. EXAFS analysis revealed that site occupancy and surface precipitation are the main Pb uptake mechanisms on clinoptilolite in the presence and absence of MTBE. The surface "embedded" Pb uptake, through the Mg site on the clinoptilolite surface, comprises a secondary mechanism of Pb binding in the presence of MTBE.

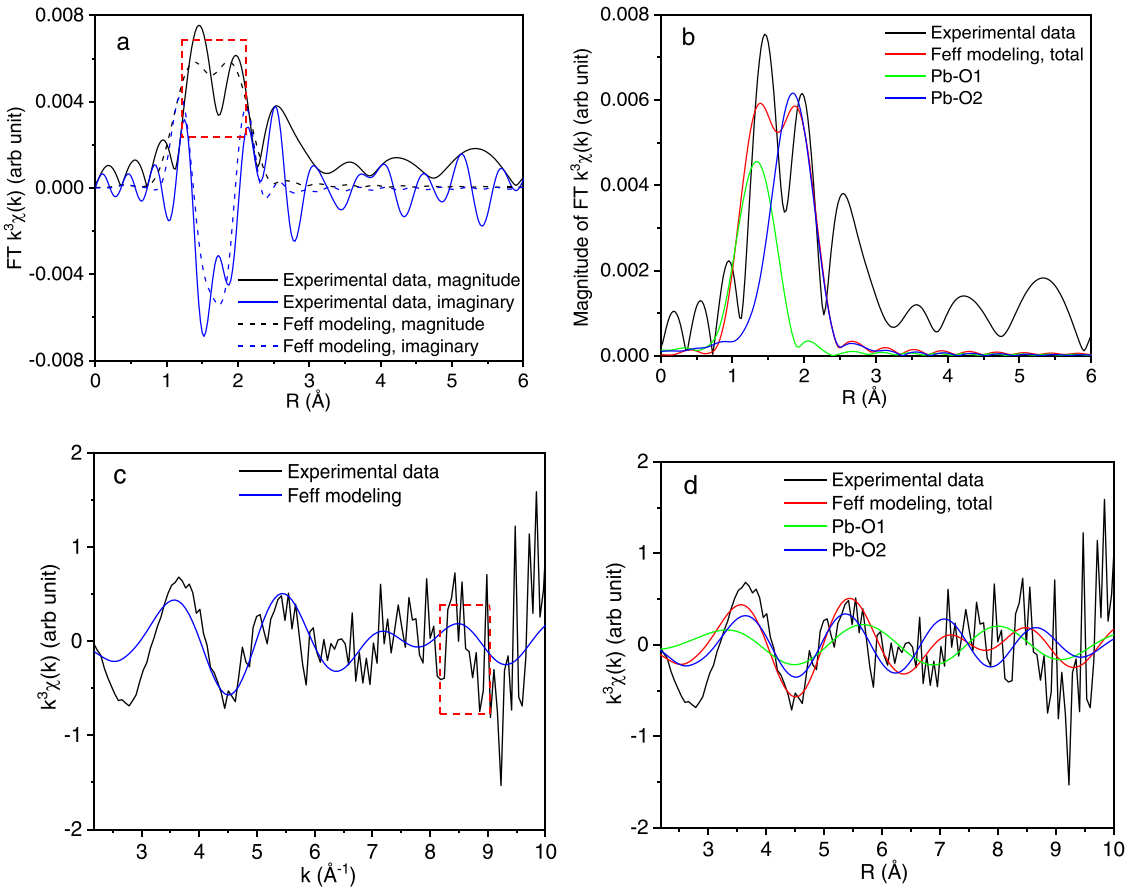

Fig. 5. Comparison of experimental data for Pb sorption onto clinoptilolite at pH 6 in the presence of MTBE and Feff modeling based fit by the M-4 model in terms of magnitude of FT and the imaginary part of the FT (a) and $k^3\chi(k)$ (c); Comparison among the magnitude of FT of experimental data, total Feff for all fitted scattering paths and Feff for each individual scattering paths (b) and experimental data, R space fitting based total Feff modeling and each fitted individual scattering path (d).

Table 4
M-4 model and R space curve fitting for Pb sorption onto clinoptilolite at pH 6 in the presence of MTBE.

Paths	M-4 model		M-4 model-based fitting		
	CN	R (Å)	CN	R (Å)	σ^2 (Å^2)
Pb-O1	4	1.57	No fitting solution		
Pb-O2	4	1.68	0.3	1.82	0.0050
Pb-O3	4	2.18	1.5	2.42	0.0100

3.4. Comparison of Pb sorption onto the two zeolites

Zeolites are generally classified as either hydrophilic or hydrophobic according to their surface properties, and this plays a significant role in the selection of zeolites for the removal of different adsorbates. In order to better understand the sorption characteristics and binding mechanisms of Pb on hydrophilic and hydrophobic zeolites, we compared hydrophilic clinoptilolite and hydrophobic ZSM-5, the latter of which was previously studied (Zhang et al., 2021b).

Pb sorption required different isotherm models for each of the minerals, a Langmuir model being a better fit for ZSM-5 and a Freundlich

Table 5
Comparison of the physicochemical properties of ZSM-5 and clinoptilolite and their sorption of Pb.

		ZSM-5	Clinoptilolite
Hydrophobicity		Hydrophobic	Hydrophilic
Contact angle		51.5 ± 4.5°	25.0 ± 0.7°
CEC		1.81 cmol/kg	180 cmol/kg
SiO_2/Al_2O_3 ratio		469	6
pH		4.1	6.7
Sorption isotherms		Langmuir	Freundlich
Sorption capacity		14.4 ± 5.8 mg/g at pH 4 46.3 ± 6.3 mg/g at pH 6	95.5 ± 15.9 mg/g at pH 4 108.3 ± 12.9 mg/g at pH 6
Influencing factor	Solution pH	Increased with the increasing pH from 4 to 6	
	Co-contaminating MTBE	Can hardly affect the Pb sorption	
Binding mechanism	In the absence of MTBE	The $PbO\bullet(H_2O)$ type of surface coating (main) and Pb to Si surface site occupancy (secondary)	Site occupancy and surface precipitation
	In the presence of MTBE	N.A.	Site occupancy and surface precipitation (main); the surface "embedded" Pb uptake through the Mg site on the surface (secondary)

N.A.: Not applicable

model for clinoptilolite (Table 5). The Pb sorption capacity of clinoptilolite was higher than ZSM-5 at both pH 4 and 6, by 81 and 62 mg/g, respectively. This is attributed to their different CEC values, which are directly related to metal adsorption. Both zeolites have a higher sorption capacity at pH 6 than at pH 4 mainly due to the surface precipitation of Pb^{2+} to form $Pb(OH)_2$ solids. This also explains why Pb sorption increased with increasing solution pH from 4 to 6 for both zeolites. The effect of co-contaminating MTBE on Pb sorption was negligible for both zeolites probably because the adsorption of MTBE and Pb onto zeolite surfaces is driven by different mechanisms: pore filling and surface complexation/precipitation, respectively. The Pb sorption mechanisms include Si surface site occupancy and the PbO•(H_2O) type of surface coating in the Pb-ZSM-5 system, with the formation of surface coatings as the main binding mechanism at pH 6. Similarly, site occupancy and surface precipitation are the main Pb uptake mechanisms on clinoptilolite in the presence and absence of MTBE. However, the surface-embedded Pb uptake at the Mg site on the surface comprised a secondary mechanism in the Pb-clinoptilolite-MTBE system.

4. Environmental implications

This study compared sorption features and binding mechanisms of Pb^{2+} on a hydrophilic zeolite, clinoptilolite, with those on a hydrophobic zeolite, ZSM-5, by the combination of adsorption modeling and synchrotron-based EXAFS analysis. The Pb sorption on both zeolites increased with increasing solution pH from 4 to 6 due to enhanced PbO•(H_2O) type surface precipitation on the zeolite surface. Unlike ZSM-5 where PbO•(H_2O) type surface coating is the main Pb uptake mechanism followed by Pb to Si surface site occupancy, the EXAFS results show that both site occupancy and surface precipitation constituted the primary Pb uptake mechanisms on clinoptilolite. The surface-embedded Pb uptake at the Mg site on the clinoptilolite surface comprised a secondary mechanism when MTBE is present in the system. This study provides new insights into the Pb binding mechanisms and stability on zeolites and indicates that MTBE (100 mg/L) does not measurably impact Pb removal, which is advantageous at co-contaminated sites.

CRediT Authorship contribution Statement

Yunhui Zhang: Conceptualization, Methodology, Investigation, Writing – Original Draft, Writing – Review & Editing. **Daniel S. Alessi:** Conceptualization, Methodology, Writing – Review & Editing, Supervision, Resources, Funding Acquisition. **Ning Chen:** Conceptualization, Methodology, Investigation, Writing – Review & Editing, Resources. **Mina Luo:** Conceptualization, Methodology, Supervision. **Weiduo Hao:** Methodology, Investigation, Writing – Review & Editing. **Md. Samrat Alam:** Methodology, Investigation. **Shannon L. Flynn:** Writing – Review & Editing. **Janice P. L. Kenney:** Writing – Review & Editing. **Kurt O. Konhauser:** Writing – Review & Editing, Resources, Funding Acquisition. **Yong Sik Ok:** Writing – Review & Editing. **Abir Al-Tabbaa:** Resources, Supervision, Project Administration.

Declaration of Competing Interest

The authors declare that they have no known competing financial interests or personal relationships that could have appeared to influence the work reported in this paper.

Acknowledgments

The first author is grateful to the China Scholarship Council (CSC) for a PhD studentship. This study was financially supported by the Natural Sciences and Engineering Research Council of Canada (NSERC) Discovery grants to DSA (RGPIN-04134) and KOK (RGPIN-165831).

Appendix A. Supporting information

Supplementary data associated with this article can be found in the online version at doi:10.1016/j.jhazmat.2021.126528.

References

Aghazadeh, S., Safarzadeh, E., Gharabaghi, M., Irannajad, M., 2016. Modification of natural zeolite for Cu removal from waste waters. Desalin. Water Treat. 1–8. https://doi.org/10.1080/19443994.2016.1183230.

Alessi, D., Flynn, S., Alam, M., Robbins, L., Konhauser, K., 2019a. Potentiometric Titrations to Characterize the Reactivity of Geomicrobial Surfaces, Kenney, J.P.L.

Alessi, D.S., Flynn, S.L., Alam, M.S., Robbins, L.J., Konhauser, K.O., 2019b. Potentiometric titrations to characterize the reactivity of geo-microbial surfaces. In: Analytical Geomicrobiology: A Handbook of Instrumental Techniques. Cambridge University Press, Cambridge, pp. 79–92.

Alghunaim, A., Kirdponpattara, S., Newby, B.M.Z., 2016. Techniques for determining contact angle and wettability of powders. Powder Technol. 287, 201–215. https://doi.org/10.1016/j.powtec.2015.10.002.

Anderson, M.W., Klinowski, J., 1986. Zeolites treated with silicon tetrachloride vapour. Part 1.- Preparation and characterisation. J. Chem. Soc., Faraday Trans. 82, 1449–1469. https://doi.org/10.1039/F19868201449.

Arjoon, A., Olaniran, A.O., Pillay, B., 2013. Enhanced 1,2-dichloroethane degradation in heavy metal co-contaminated wastewater undergoing biostimulation and bioaugmentation. Chemosphere 93, 1826–1834. https://doi.org/10.1016/J.CHEMOSPHERE.2013.06.034.

Duc, M., Gaboriaud, F., Thomas, F., 2005. Sensitivity of the acid–base properties of clays to the methods of preparation and measurement: 2. Evidence from continuous potentiometric titrations. J. Colloid Interface Sci. 289, 148–156. https://doi.org/10.1016/J.JCIS.2005.03.057.

EPA, 2006. Aquatic life criteria - Methyl tertiary-butyl ether (MTBE) [WWW Document]. URL ⟨https://www.epa.gov/wqc/aquatic-life-criteria-methyl-tertiary-butyl-ether-mtbe⟩.

Erdem-Şenatalar, A., Bergendahl, J.A., Giaya, A., Thompson, R.W., 2004. Adsorption of Methyl Tertiary Butyl Ether onHydrophobic Molecular Sieves. Environ. Eng. Sci. 21 (6), 722–729. https://doi.org/10.1089/ees.2004.21.722.

Filippousi, M., Turner, S., Katsikini, M., Pinakidou, F., Zamboulis, D., Pavlidou, E., Van Tendeloo, G., 2015. Direct observation and structural characterization of natural and metal ion-exchanged HEU-type zeolites. Microporous Mesoporous Mater. 210, 185–193. https://doi.org/10.1016/j.micromeso.2015.01.043.

Förch, R., Schönherr, H., Jenkins, A.T.A., 2009. Surface design: Applications in bioscience and nanotechnology. https://doi.org/10.1002/9783527628599.

Global Industry Analysts, I., 2019. Methyl tert-butyl ether (MTBE) - Market analysis, trends, and forecasts by global industry analysts, Inc. [WWW Document].

Hao, W., Flynn, S.L., Alessi, D.S., Konhauser, K.O., 2018. Change of the point of zero net proton charge (pH_{PZNPC}) of clay minerals with ionic strength. Chem. Geol. 493, 458–467. https://doi.org/10.1016/J.CHEMGEO.2018.06.023.

Hao, W., Flynn, S.L., Kashiwabara, T., Alam, M.S., Bandara, S., Swaren, L., Robbins, L.J., Alessi, D.S., Konhauser, K.O., 2019. The impact of ionic strength on the proton reactivity of clay minerals. Chem. Geol. 529, 119294 https://doi.org/10.1016/J.CHEMGEO.2019.119294.

Hao, W., Kashiwabara, T., Jin, R., Takahashi, Y., Gingras, M., Alessi, D.S., Konhauser, K.O., 2020. Clay minerals as a source of cadmium to estuaries. Sci. Rep. 10, 10417. https://doi.org/10.1038/s41598-020-67279-w.

Herbelin, A., Westall, J., 1996. FITEQL-A computer program for determination of chemical equilibrium constants from experimental data version 3.2 user's manual. Corvallis, OR.

Izumi, Y., Kiyotaki, F., Minato, T., Seida, Y., 2002. X-ray absorption fine structure combined with fluorescence spectrometry for monitoring trace amounts of lead adsorption in the environmental conditions. Anal. Chem. 74 (15), 3819–3823. https://doi.org/10.1021/ac025550p.

Jiang, D.T., Chen, N., Sheng, W., 2007. Wiggler-base hard X-ray spectroscopy beamline at CLS, in: Choi, JY and Rah, S. (Ed.), AIP Conference Proceedings, AIP Conference Proceedings. pp. 800–803.

Joly, Y., 2001. X-ray absorption near-edge structure calculations beyond the muffin-tin approximation. Phys. Rev. B 63, 125120. https://doi.org/10.1103/PhysRevB.63.125120.

Karatas, M., 2012. Removal of Pb(II) from water by natural zeolitic tuff: Kinetics and thermodynamics. J. Hazard. Mater. 199–200, 383–389. https://doi.org/10.1016/J.JHAZMAT.2011.11.035.

Krauklis, A., Ozola, R., Burlakovs, J., Rugele, K., Kirillov, K., Trubaca-Boginska, A., Rubenis, K., Stepanova, V., Klavins, M., 2017. FeOOH and Mn8O10Cl3 modified zeolites for As(V) removal in aqueous medium. J. Chem. Technol. Biotechnol. 92, 1948–1960. https://doi.org/10.1002/jctb.5283.

Li, Z., Alessi, D., Allen, L., 2002. Influence of quaternary ammonium on sorption of selected metal cations onto clinoptilolite zeolite. J. Environ. Qual. 31, 1106–1114. https://doi.org/10.2134/jeq2002.1106.

Liu, J., Pan, J., Ma, Y., Liu, S., Qiu, F., Yan, Y., 2018a. A versatile strategy to fabricate dual-imprinted porous adsorbent for efficient treatment co-contamination of λ-cyhalothrin and copper(II). Chem. Eng. J. 332, 517–527. https://doi.org/10.1016/J.CEJ.2017.09.079.

Liu, Y., Alessi, D.S., Flynn, S.L., Alam, M.S., Hao, W., Gingras, M., Zhao, H., Konhauser, K.O., 2018b. Acid-base properties of kaolinite, montmorillonite and illite

at marine ionic strength. Chem. Geol. 483, 191–200. https://doi.org/10.1016/J.CHEMGEO.2018.01.018.
Logar, N.Z., Šiljeg, M., Arčon, I., Meden, A., Tušar, N.N., Štefanović, Š.C., Kovač, J., Kaučič, V., 2006. Sorption of Cr^{3+} on clinoptilolite tuff: a structural investigation. Microporous Mesoporous Mater. 93 (1–3), 275–284. https://doi.org/10.1016/j.micromeso.2006.02.026.
Mihaly-Cozmuta, L., Mihaly-Cozmuta, A., Peter, A., Nicula, C., Tutu, H., Silipas, D., Indrea, E., 2014. Adsorption of heavy metal cations by Na-clinoptilolite: equilibrium and selectivity studies. J. Environ. Manag. 137, 69–80. https://doi.org/10.1016/J.JENVMAN.2014.02.007.
Ozola, R., Krauklis, A., Burlakovs, J., Klavins, M., Vincevica-Gaile, Z., Hogland, W., 2019. Surfactant-modified clay sorbents for the removal of p-nitrophenol. Clays Clay Min. 67, 132–142. https://doi.org/10.1007/s42860-019-00015-2.
Ravel, B., Newville, M., 2005. Athena, Artemis, Hephaestus: data analysis for X-ray absorption spectroscopy using IFEFFIT. J. Synchrotron Radiat. 12, 537–541. https://doi.org/10.1107/S0909049505012719.
Rehr, J.J., Albers, R.C., 2000. Theoretical approaches to x-ray absorption fine structure. Rev. Mod. Phys. 72, 621–654. https://doi.org/10.1103/RevModPhys.72.621.
Ressler, T., 1997. WinXAS: a new software package not only for the analysis of energy-dispersive XAS data. Le. J. Phys. IV 7, C2–269-C2-270. https://doi.org/10.1051/jp4/1997195.
Shen, Z., Jin, F., Wang, F., McMillan, O., Al-Tabbaa, A., 2015. Sorption of lead by Salisbury biochar produced from British broadleaf hardwood. Bioresour. Technol. 193, 553–556. https://doi.org/10.1016/j.biortech.2015.06.111.
Sprynskyy, M., Buszewski, B., Terzyk, A.P., Namieśnik, J., 2006. Study of the selection mechanism of heavy metal (Pb^{2+}, Cu^{2+}, Ni^{2+}, and Cd^{2+}) adsorption on clinoptilolite. J. Colloid Interface Sci. 304, 21–28. https://doi.org/10.1016/j.jcis.2006.07.068.
Tolkachev, S.S., Stroganov, E.V., Kozhina, I.I., 1958. The structure of lead oxide monohydrate. Vestn. Leningr. Univ. Ser. Fiz. Khim 16, 134–139.
Um, W., Papelis, C., 2003. Sorption mechanisms of Sr and Pb on zeolitized tuffs from the Nevada test site as a function of pH and ionic strength. Am. Mineral. 88, 2028–2039.
Wang, S., Peng, Y., 2010. Natural zeolites as effective adsorbents in water and wastewater treatment. Chem. Eng. J. 156, 11–24. https://doi.org/10.1016/j.cej.2009.10.029.
Yuna, Z., 2016. Review of the natural, modified, and synthetic zeolites for heavy metals removal from wastewater. Environ. Eng. Sci. 33, 443–454. https://doi.org/10.1089/ees.2015.0166.
Zhang, L., Qian, L., Ding, L., Wang, L., Wong, M.H., Tao, H., 2021a. Ecological and toxicological assessments of anthropogenic contaminants based on environmental metabolomics. Environ. Sci. Ecotechnol. 5, 100081 https://doi.org/10.1016/j.ese.2021.100081.
Zhang, Y., Alessi, D.S., Chen, N., Luo, M., Hao, W., Alam, M.S., Konhauser, K.O., Ok, Y.S., Al-Tabbaa, A., 2021b. Spectroscopic and modeling investigation of sorption of Pb(II) to ZSM-5 zeolites. ACS ES&T Water 1, 108–116. https://doi.org/10.1021/acsestwater.0c00010.
Zhang, Y., Hou, D., O'Connor, D., Shen, Z., Shi, P., Ok, Y.S., Tsang, D.C.W., Wen, Y., Luo, M., 2019a. Lead contamination in Chinese surface soils: source identification, spatial-temporal distribution and associated health risks. Crit. Rev. Environ. Sci. Technol. 49, 1386–1423. https://doi.org/10.1080/10643389.2019.1571354.
Zhang, Y., Jin, F., Shen, Z., Lynch, R., Al-Tabbaa, A., 2018a. Kinetic and equilibrium modelling of MTBE (methyl tert-butyl ether) adsorption on ZSM-5 zeolite: batch and column studies. J. Hazard. Mater. 347, 461–469. https://doi.org/10.1016/J.JHAZMAT.2018.01.007.
Zhang, Y., Jin, F., Shen, Z., Wang, F., Lynch, R., Al-Tabbaa, A., 2019b. Adsorption of methyl tert-butyl ether (MTBE) onto ZSM-5 zeolite: fixed-bed column tests, breakthrough curve modelling and regeneration. Chemosphere 220, 422–431. https://doi.org/10.1016/j.chemosphere.2018.12.170.
Zhang, Y., Wu, L., Huang, P., Shen, Q., Sun, Z., 2018b. Determination and application of the solubility product of metal xanthate in mineral flotation and heavy metal removal in wastewater treatment. Miner. Eng. 127, 67–73. https://doi.org/10.1016/J.MINENG.2018.07.016.
Zhang, Y., 2019. Characteristics and Mechanisms of Heavy Metal and MTBE Adsorption on Zeolites and Applications in Permeable Reactive Barriers. University of Cambridge, Cambridge, U.K.. https://doi.org/10.17863/CAM.45900. Ph.D. Dissertation.